Structure Functions in Deep Inelastic Lepton-Nucleon Scattering

Max Klein
DESY/Zeuthen
Platanenallee 6
D-15738 Zeuthen, Germany

This report presents the latest results on structure functions, as available at the Lepton-Photon Symposium 1999. It focuses on three experimental areas: new structure function measurements, in particular from HERA at low x and high Q^2; results on light and heavy flavor densities; and determinations of the gluon distribution and of α_s. As the talk was delivered at a historic moment and place, a few remarks were added recalling the exciting past and looking into the promising future of deep inelastic scattering (DIS).

1 Introduction

About three decades ago, highly inelastic electron-proton scattering was observed by a SLAC-MIT Collaboration [1], which measured the proton structure function $\nu W_2(Q^2, \nu)$ to be independent of the four-momentum transfer squared Q^2 at fixed Bjorken $x = Q^2/2M_p\nu$. Here, $\nu = E - E'$ is the energy transferred by the virtual photon. It is related to the inelasticity y through $\nu = sy/2M_p$, with proton mass M_p and the energy squared in the center of mass system $s = 2M_pE$. With the SLAC linear accelerator, the incoming electron energy E had been successfully increased by a factor of twenty as compared to previous form factor experiments [2]. Thus, $Q^2 = 4EE'\sin^2(\theta/2)$ could be enlarged and measured using the scattered electron energy E' and its polar angle θ. Partonic proton substructure [3] was established at $1/\sqrt{Q^2} \simeq 10^{-16}$ m, and this allowed the scaling behavior [4] of $\nu W_2(Q^2, \nu) \to F_2(x)$ to be interpreted. In the quark-parton model (QPM) [5], the structure function F_2 is given by the momentum distributions of valence and sea quarks, $q = q_v + q_s$, and of antiquarks $\overline{q}$ weighted by the square Q_q^2 of the electric charge,

$$F_2(x, Q^2) = x \sum_q Q_q^2 (q + \overline{q}) \ . \tag{1}$$

Neutrino experiments found $\sigma_\nu \simeq 3\, \sigma_{\overline{\nu}}$, demonstrating that partons could be identified with quarks having gauge couplings like leptons and that, at large x, the sea is small. Scaling violations were hidden in the first DIS data taken at $x \simeq 0.2$, as if we

needed help to understand the basics of inelastic scattering. They were found in μN scattering [6] in an extended x, Q^2 range. The logarithmic Q^2 dependence of $F_2(x, Q^2)$, established in subsequent neutrino and muon-nucleon scattering experiments, was attributed to quark-gluon interactions in Quantum Chromodynamics [7].

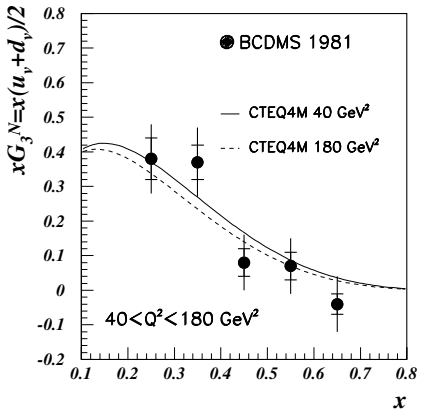

Figure 1: Measurement of the γZ interference structure function xG_3 in $\mu^{\pm}$ Carbon scattering by the BCDMS Collaboration [12] compared with a recent parametrization of the valence quark distributions by the CTEQ group.

With the discovery of neutral currents [8], DIS neutrino experiments made a major contribution to the theory of weak interactions. In 1979, another ep scattering experiment was performed at SLAC [9] which determined, in a highly sensitive polarization asymmetry measurement at $Q^2 \simeq 1.5$ GeV^2, that the right-handed weak isospin charge of the electron was zero. This experiment selected the Glashow-Weinberg-Salam model as the standard electroweak theory and opened the possibility of investigating proton structure at high Q^2 via Z boson exchange. The nucleon structure function F_2 was generalized, still in a $V-A$ theory [10], to three functions

$$(F_2, G_2, H_2) = x \sum_q (Q_q^2, 2Q_q v_q, v_q^2 + a_q^2)(q + \overline{q}) \tag{2}$$

arising from photon exchange (F_2), γZ interference (G_2), and Z exchange (H_2), where $v_q(a_q)$ are the vector (axial vector) quark couplings [11]. In charged lepton-nucleon neutral current (NC) scattering, two further structure functions appear which are analogous to xF_3 in neutrino scattering

$$(xG_3, xH_3) = 2x \sum_q (Q_q a_q, v_q a_q)(q - \overline{q}). \tag{3}$$

A DIS muon experiment with simultaneous beam charge and polarity reversal resulted in the first determination of the γZ interference structure function xG_3 at $Q^2 \simeq 60$ GeV^2 by the BCDMS Collaboration at CERN [12] (Fig. 1). Electroweak

interference occurs at the level of $\kappa \simeq 10^{-4} Q^2/\ \mathrm{GeV}^2$, as defined by the ratio of the weak and the electromagnetic coupling constants. Because the axial vector couplings could be considered to be known, this was an interesting measurement of the valence quark distribution sum $u_v + d_v$, which confirmed the sign of the quark charge combination $Q_u - Q_d$ to be positive.

With the HERA energy of $s = 4E_eE_p \simeq 10^5\ \mathrm{GeV}^2$, the kinematic range of DIS experiments could be greatly extended towards high Q^2, because s was enlarged by a factor of about $2E_p/\mathrm{GeV}$ compared to fixed target scattering. The first measurements of F_2 by the H1 [13] and the ZEUS [14] Collaborations, using data taken in 1992, reached $x \simeq 0.0005$ at $Q^2 \simeq 20\ \mathrm{GeV}^2$. They discovered a steep rise of $F_2(x, Q^2)$ towards low x at fixed Q^2: below $x \simeq 0.01$ a decrease by one order of magnitude translates into an increase of F_2 by about a factor of two (Fig. 2). Although the

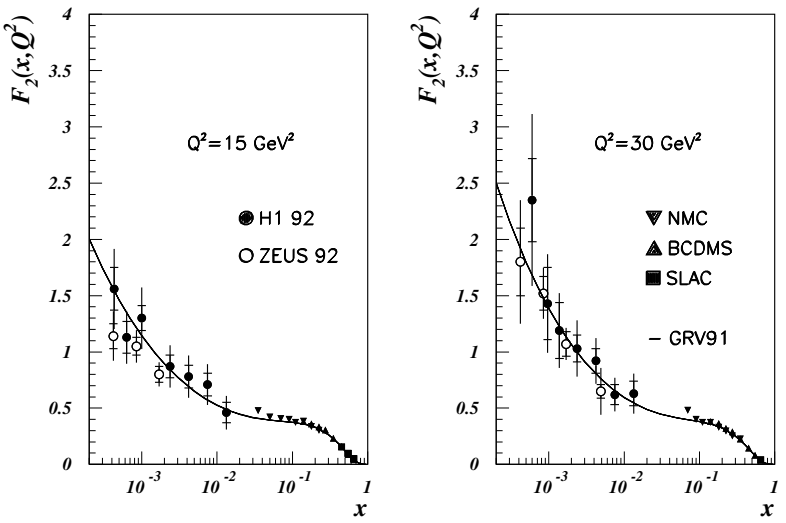

Figure 2: Measurements of the proton structure function $F_2(x, Q^2)$ by the muon-proton scattering experiments BCDMS and NMC and their extension towards low x by the first available HERA data on F_2. The curve represents the anticipation of this rising behavior by Glück, Reya, and Vogt [17].

"Possible Non-Regge Behavior of Electroproduction Structure Functions" [15] at low x had been considered and the concept [16] and modified phenomenology [17] of 'dynamical partons' had been worked out, this rise came as some surprise because the DGLAP evolution equations do not *a priori* fix the x behavior. This rise is now basically understood as being due to the dominance of gluons which leads to scaling violations described by $\partial F_2/\partial \ln Q^2 \sim \alpha_s \cdot xg$ for $Q^2 \gg M_p^2$ and low x. Its quantitative description in NLO QCD and the search for new dynamics [18] connected with large logarithms of $1/x$ requires the highest possible precision, *i.e.*, improved

instrumentation and higher luminosity than was available when the first observation was made.

While much attention has been paid to the inclusive and charm structure function measurements at HERA, remarkable progress was also achieved in the investigation of up, down, strange, and charm quark distributions with neutrino and Drell-Yan experiments at the Tevatron.

This paper describes a talk on structure functions in deep inelastic scattering delivered in 1999. Such a report is to some extent personal and cannot possibly cover this expanding field of particle physics in any exhaustive fashion. It thus may be seen together with further articles, *e.g.* [19, 20], and with the conference on deep inelastic scattering and QCD held at Zeuthen in April 1999 [21]. It demonstrates remarkable progress in DIS since the previous Symposium on Lepton-Photon Interactions [22]. This talk focused on recent measurements of structure functions (Section 2), of quark distributions including charm (Section 3) and determinations of the gluon distribution and of α_s (Section 4). The field of deep inelastic lepton-nucleon scattering has an exciting future, as will be described briefly in Section 5.

2 Recent measurements of structure functions

Since the first SLAC experiment, fixed target muon and neutrino-nucleon scattering experiments and subsequently the HERA collider experiments H1 and ZEUS extended the explored kinematic region of DIS by several orders of magnitude (Fig. 3). At the smallest x, partons carry only a vanishing fraction of the proton momentum. Hence, the kinematics resembles the fixed target experiments where both the electron and hadrons are scattered into the lepton beam direction (unfortunately termed 'backward' at HERA). For high $Q^2 > sxE_e/(E_e + xE_p)$, *i.e.* $Q^2 > 2800$ GeV^2 for $x > 0.5$, the electron is scattered through angles $\theta > 90^o$ with respect to the electron beam direction, similar to Rutherford backscattering. The kinematic range of the HERA collider experiments is confined to about $y \geq 0.001$. For lower y, hadrons escape in the forward (proton beam) direction. At very small y, the inclusive kinematics cannot be reliably reconstructed using the scattered electron variables alone, because the x resolution varies like $1/y$.

Until 1997, HERA ran with positrons scattered off protons of 820 GeV energy and about 40 pb^{-1} of luminosity became available for each collider experiment. From 1998 till May 1999, data samples of about 15 pb^{-1} were collected in collisions of electrons with 920 GeV protons. The $e^{\pm}$ energy is tuned to about 27.5 GeV to optimize the polarization for the fixed target experiment HERMES. Longitudinal lepton beam polarization is foreseen to be used in colliding beam mode from 2001 onwards.

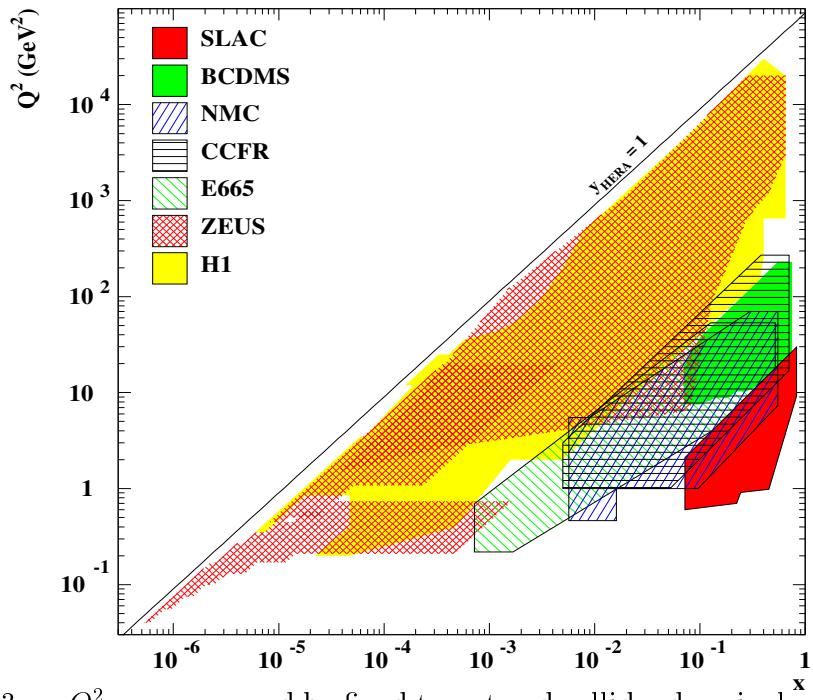

Figure 3: x, Q^2 range covered by fixed target and collider deep inelastic neutral current scattering experiments carried out until 1997.

2.1 Transition to photoproduction and low $Q^2 \leq M_p^2$

The structure function F_2 which dominates the DIS cross section behaves like $x^{-\lambda(x,Q^2)}$ and vanishes due to gauge invariance with $Q^2 \to 0$ like $\mathrm{O}(Q^2)$. The total virtual photon-proton scattering cross section is related to F_2 as $\sigma_{tot}^{\gamma^* p} \simeq 4\pi^2\alpha \cdot F_2/Q^2$. Measurements of F_2 at low Q^2 investigate the dynamics of the transition from the deep inelastic to the photoproduction regime [23]. In Regge theory, the structure function F_2 results from a superposition of exchanged Regge poles with intercepts α_i, $F_2 = \sum \beta_i(Q^2) W^{2\alpha_i - 2}$, where W is the invariant mass of the $\gamma^* p$ system and $W^2 \simeq Q^2/x \gg Q^2$ for low x. A recent fit to F_2 data (DL98) is rather successful using three trajectories, $\alpha_1 = 1.08$ for the soft pomeron, $\alpha_2 = 0.55$ for a and f exchange, and $\alpha_3 = 1.4$ for the so-called hard pomeron [24]. For $Q^2 \to 0$, the exponent λ is approximately given by the dominant pomeron Regge trajectory, *i.e.*, $\lambda \simeq \alpha_1 - 1 \simeq 0.1$. The recent ZEUS data [25], obtained with a backward calorimeter and tracker positioned close to the beam pipe, are rather well described by this model (Fig. 4). Phenomenological models using a combination of Generalized Vector Meson Dominance [26] and perturbative QCD [27] also describe this transition well. Extrapolations of $F_2(x, W^2)$ to $Q^2 \simeq 0$ come out to be somewhat higher than the direct measurements of $\sigma_{tot}^{\gamma^* p}$ [25] with tagged electrons. The F_2 based $\sigma_{tot}^{\gamma^* p}$ data are

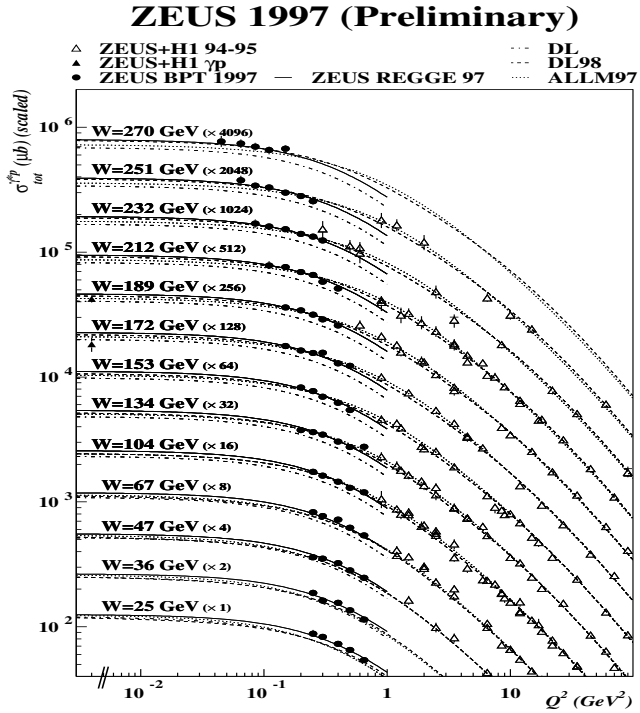

Figure 4: Measurements of the proton structure function $F_2(x, Q^2)$ expressed as $\sigma_{tot}^{\gamma^* p}(Q^2, W^2)$ from recent low Q^2 data by ZEUS (closed points) and rebinned F_2 data at larger Q^2 by H1 and ZEUS (open squares). The two triangles at $W = 172$ GeV and $W = 189$ GeV near $Q^2 \approx 0$ denote the direct photoproduction cross section measurements of H1 and ZEUS.

still at some distance in Q^2 from the real photoproduction measurements, which have uncertainties of about 10% due to beam optics and the imperfect simulation of the complete final state. Further extension of the range of the inclusive F_2 measurements at HERA towards lowest Q^2 values is thus desirable. This could be achieved in a rather short run of HERA at minimum possible electron beam energy, because Q^2 is proportional to E^2 for all except the high y values.

New data on parton-hadron duality [28] became available this year from an experiment at Jefferson Laboratory [29] measuring electron-proton and deuteron scattering in the resonance region $W \simeq 1$ GeV. The superposition of cross sections, determined at different Q^2 between 0.2 and 3.3 GeV^2, leads to an averaged behavior of F_2 which is valence-like even at low x, or mass corrected ξ [30], which supports the assumption made in the GRV analysis [17] for the initial x distributions at very small Q^2. In this experiment, which in the future will measure the ratio $R = \sigma_L/\sigma_T$, one estimates power corrections ('higher twists') to be small and derives the magnetic elastic proton

form factor G_M^p from inelastic data.

2.2 Neutrino experiments

The final measurement of νFe and $\overline{\nu} Fe$ scattering cross sections by the CCFR Collaboration [31] is in good agreement with previous data obtained by the CDHSW Collaboration and is more accurate. The high statistics CCFR data has been used for a number of investigations regarding all structure functions involved (Sections 2.3, 2.4) and also for tests of QCD (Section 4.3). Recently, data were released for extremely large x ($x > 0.75$), pointing to cumulative effects beyond Fermi motion in the nucleus [32] which were studied previously by the BCDMS Collaboration [33].

Data were obtained by the IHEP-JINR neutrino experiment in the wide band neutrino beam at the Serpukhov U70 accelerator [34]. Based on about 750 ν and 6000 $\overline{\nu}$ events for $W^2 > 1.7$ GeV^2 and $Q^2 \simeq 2$ GeV^2, the structure functions F_2 and xF_3 were disentangled and $\alpha_s(M_Z^2) = 0.123^{+0.010}_{-0.013}$ was determined in NLO QCD.

2.3 Precision measurement at low x and medium Q^2

The H1 Collaboration released for this conference the most precise measurement so far of the DIS cross section at HERA. This cross section is written in its reduced form as

$$\frac{Q^4 x}{2\pi\alpha^2 Y_+} \cdot \frac{d^2\sigma}{dQ^2 dx} = \sigma_r = F_2 - \frac{y^2}{Y_+} \cdot F_L, \tag{4}$$

so that $\sigma_r \simeq F_2$ apart from high y where $\sigma_r \to F_2 - F_L \propto \sigma_T$. Here F_L denotes the longitudinal structure function, which is related to the ratio $R = F_L/(F_2 - F_L)$, and $Y_+ = 1 + (1-y)^2$. The H1 data, taken in 1996 and 1997, have statistical errors of typically 1% and systematic errors of 2-3%, apart from edges of the acceptance region. In order to reach this precision, HERA has been annually increasing the luminosity. The H1 experiment was subject to a major upgrade of its backward apparatus, replacing a Pb-Scintillator calorimeter with a Pb-fiber calorimeter of higher granularity and an MWPC with a planar drift chamber, and adding a high resolution Silicon strip detector telescope for electron track identification and kinematic reconstruction. This upgrade permitted the measurement to be extended to high $y \leq 0.89$ in order to access F_L (Section 2.4) and to low $y \geq 0.003$ in order to reach the x range covered by DIS fixed target experiments. Comparing the data shown in Fig. 5 with the initial HERA data, Fig. 2, one recognizes the impressive progress made in a few years. The data are well described by NLO QCD as discussed in Section 4.2. Consistent results on preliminary F_2 data were previously obtained by the H1 and ZEUS Collaborations [35].

The H1 data help in resolving a long standing controversy between the NMC and E665 μp data and the CCFR νN data on the structure function F_2. As shown

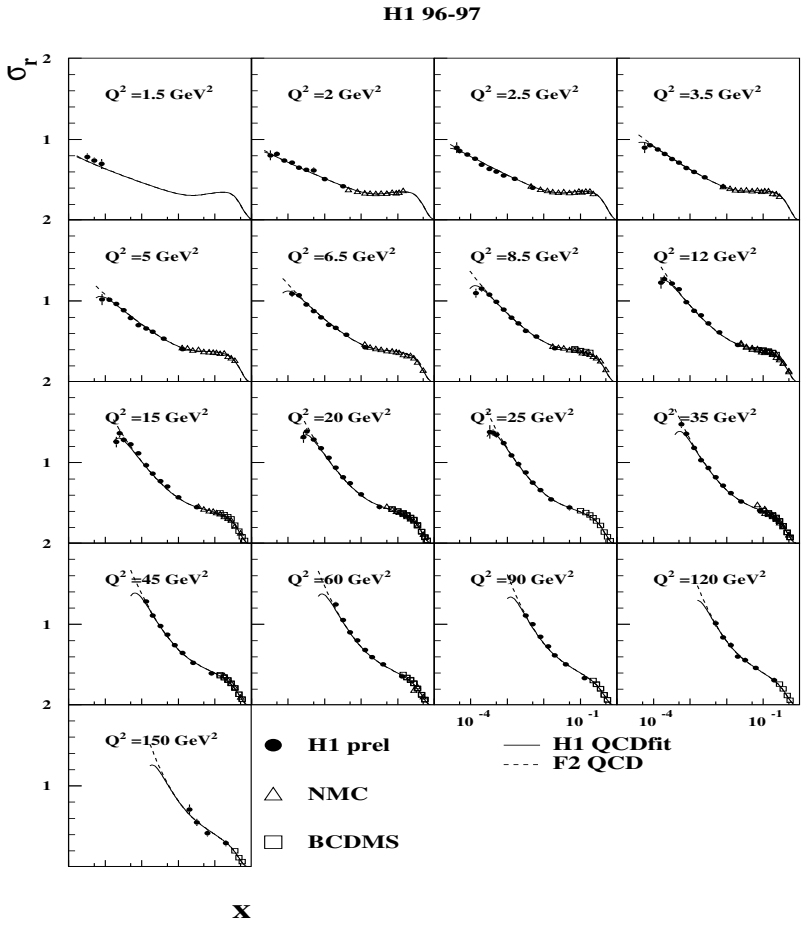

Figure 5: Measurements of the DIS cross section by H1 compared with NMC and BCDMS μp data. The solid curve denotes the fitted cross section in NLO QCD using H1 and NMC data for $Q^2 \geq 3.5$ GeV^2. The dashed curve is the structure function F_2 obtained in the QCD fit which at low x departs from σ_r.

in Fig. 6, the H1 data overlap and extrapolate well to the μp data. The CCFR F_2 determination, which is being redone [36], was recently criticized regarding the treatment of charm and shadowing [37]. Because F_2 and xF_3 add up to the measured cross section, an F_2 reanalysis may affect also the value of α_s derived from xF_3. The CCFR cross section measurement improved in a consistent way the CDHSW cross section data. Those seem not to be in contradiction with muon data [38].

Precision measurements at HERA are essential for calculating the expected rates at LHC energies and also for estimating the neutrino scattering cross sections in active galactic nuclei or gamma ray bursts at ultra high energies, up to $E_\nu \simeq 10^{12}$ GeV. Recently very high energy rates were calculated using the DGLAP equations [39], the GRV approach in DGLAP QCD [40], and a combination of DGLAP and BFKL dynamics [41]. These different approaches agree remarkably well.

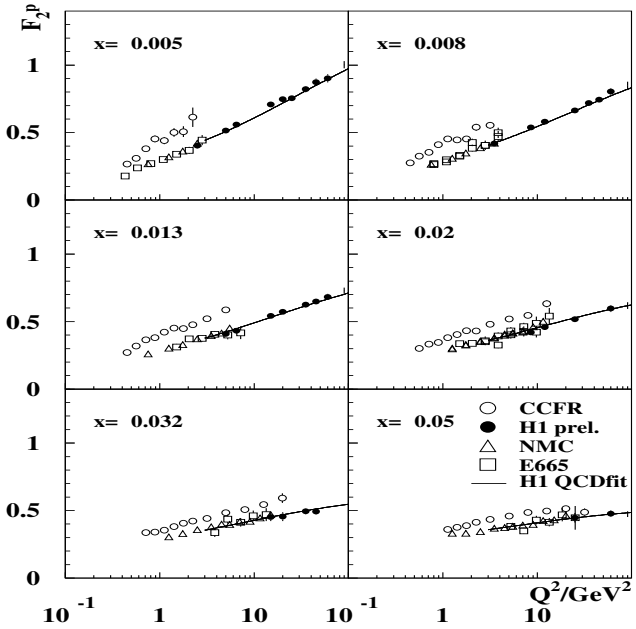

Figure 6: F_2 structure function data of CCFR, NMC, E665, and H1. The CCFR data were corrected for nuclear effects and for the difference of F_2 in charged lepton and neutrino scattering [36]. The CCFR data are shown with statistical errors only.

2.4 Longitudinal structure function F_L

In the naive QPM, the longitudinal structure function F_L is zero, because the partons have spin 1/2. In QCD, F_L acquires a possibly large value due to gluon emission and represents, together with F_2, a strong constraint to the theory in NLO.

The sum of ν and $\overline{\nu}$ nucleon scattering cross sections is proportional to $2xF_1(1+\epsilon R) - Y_- \cdot \Delta xF_3/2Y_+$ where $\epsilon = 2(1-y)/Y_+$ is the polarization of the W boson exchanged and $Y_\pm = 1 \pm (1-y)^2$. Thus, it is sensitive to R. The CCFR Collaboration has studied the Q^2 dependence of R for $0.015 \leq x \leq 0.5$ and $Q^2 < 5$ GeV^2 using phenomenological descriptions for the strange and charm quark distribution difference determined by $\Delta xF_3 \simeq 4x(s-c)$. The ratio R tends to be large, $R \geq 0.5$, at small $Q^2 \simeq 1-2$ GeV^2 and $x < 0.1$. For $Q^2 > 10$ GeV^2, the function $\Delta xF_3 = xF_3^\nu - xF_3^{\overline{\nu}}$ was extracted and this result is of interest for the treatment of massive charm [42].

Using unpolarized targets, the HERMES Collaboration measured the ratio of nitrogen to deuterium electroproduction cross sections to be astonishingly small at low Q^2 [43]. This effect has been attributed to a very large ratio $R_N/R_D \geq 5$ in the region $0.01 < x \leq 0.06$ and $0.5 \leq Q^2 < 1.5$ GeV^2, with as yet unexplained origin.

The measurements of the longitudinal structure function in ep and μp scattering are summarized in Fig. 7. The H1 data were obtained using assumptions for the behavior of F_2 in QCD (for $Q^2 > 10$ GeV^2) and, independently of QCD, for the

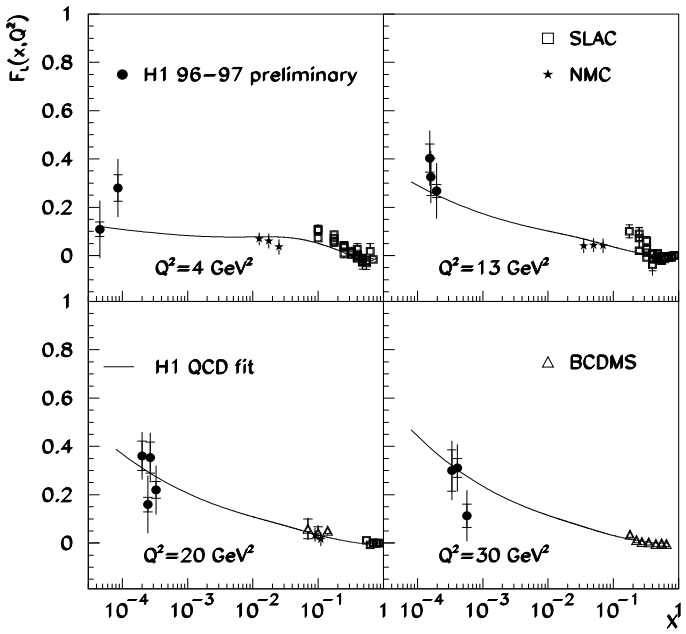

Figure 7: Measurements of the longitudinal structure function $F_L(x, Q^2)$ in ep and μp scattering. At low x, F_L is large because of dominant contributions of a large gluon momentum density. The four bins comprise data between $Q^2 = 2, 5, 15, 25$, and 50 GeV^2, respectively. The curves represent the H1 calculation of F_L.

derivative $\partial F_2/\partial \ln y$ (for $Q^2 < 10$ GeV^2) in the high y region [44] where the cross section approaches $F_2 - F_L$. Contrary to fixed target experiments, such assumptions are possible because HERA covers more than two orders of magnitude in y where F_2 can be fixed independently of F_L. The overall behavior of F_L as a function of x is well described by a QCD fit in NLO using F_2 data only, *i.e.*, by deriving the gluon (and parton) distributions from scaling violations and then calculating F_L (Fig. 7).

The behavior of R observed at low $Q^2 \simeq 1$ GeV^2 and the so far limited accuracy of the H1 F_L data, obtained with 6.8 pb^{-1}, represent a challenge for forthcoming experiments and their theoretical interpretation. This comprises the hypothesis of particularly large higher twist effects and large higher order corrections. At low x and Q^2, these corrections may even become negative due to a large negative contribution of the gluonic coefficient function [45].

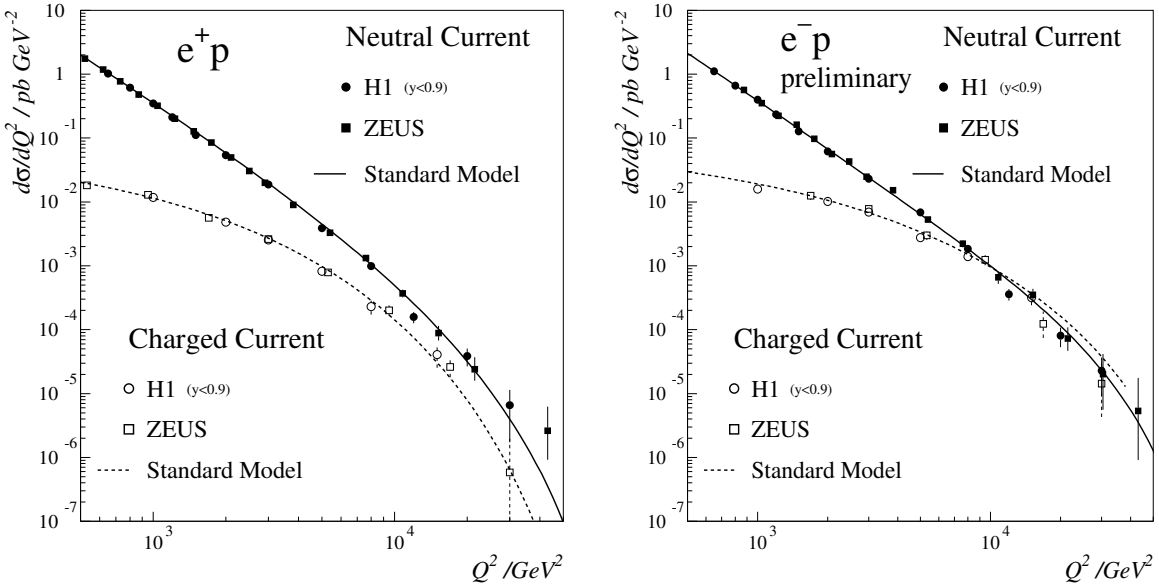

Figure 8: Measurements of the Q^2 dependence of the positron and the electron proton neutral and charged current scattering cross sections at HERA, using data taken in 1994-1997 ($e^+, E_p = 820$ GeV) and in 1998-1999 ($e^-, E_p = 920$ GeV). Electromagnetic and weak interaction cross sections become of similar strength for $Q^2 \simeq M_Z^2, M_W^2$.

2.5 Weak neutral currents at HERA

At high $Q^2 \simeq M_{W,Z}^2$, the photon, Z-boson, and W-boson exchange are of comparable strength. Thus, electroweak interactions can be used to probe proton structure in neutral (NC) and charged current (CC) scattering at HERA in the same experiments. This is demonstrated with the Q^2 distributions in electron and positron proton NC and CC scattering, Fig. 8, measured by H1 (e^+ NC, CC [46]; e^- NC, CC [47]) and by ZEUS (e^+ NC [48], e^+ CC [49], and e^- NC, CC [50]).

The double-differential NC cross section, neglecting the three longitudinal structure functions, is given by two generalized structure functions $\mathbf{F_2}$ and $\mathbf{xF_3}$

$$\frac{d^2\sigma^{\pm}}{dQ^2dx} = \sigma^{\pm} = \frac{2\pi\alpha^2}{Q^4x} \cdot [Y_+\mathbf{F_2^{\pm}} + Y_-\mathbf{xF_3^{\pm}}]. \quad (5)$$

These depend on the quark couplings and distributions, but, contrary to the hadronic tensor definitions of structure functions [10], they depend also on the weak electron

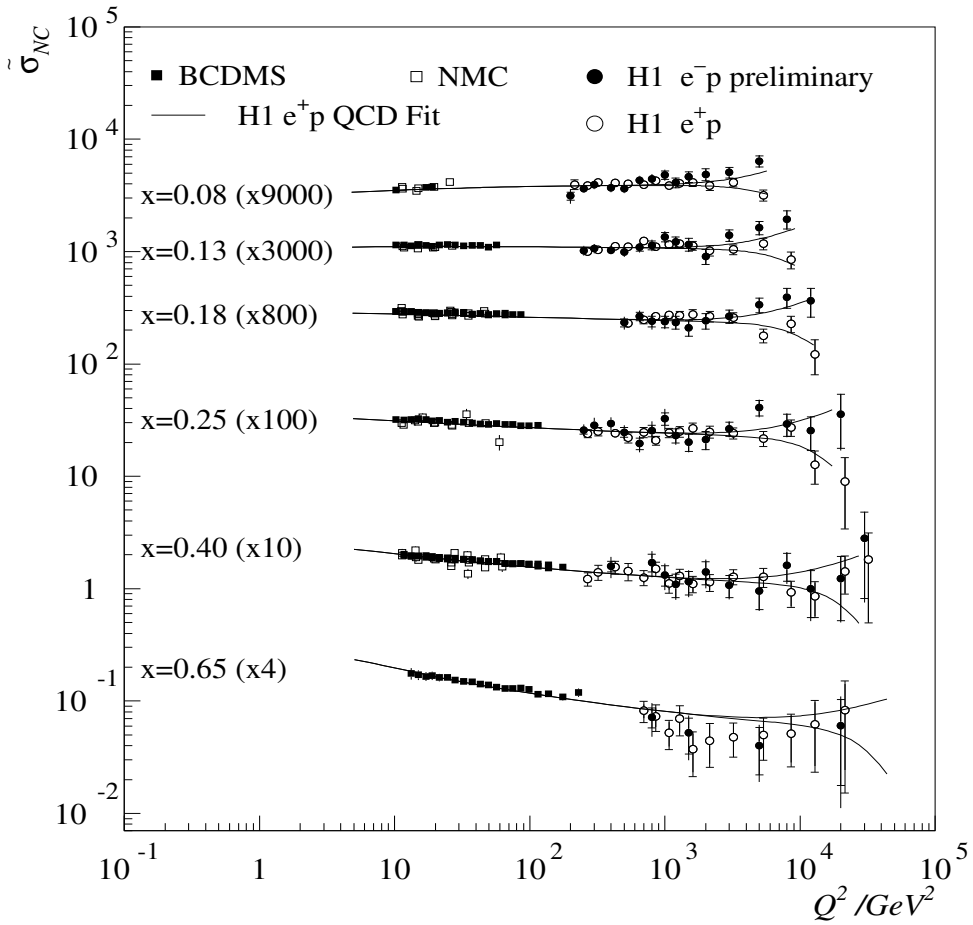

Figure 9: Measurements of the double differential NC e^+ and e^- proton scattering cross sections by H1, NMC, and BCDMS. The high Q^2 H1 data are well described by a QCD fit, which may even be restricted to $Q^2 < 150$ GeV^2 [47], representing a remarkable confirmation of the DGLAP evolution in Q^2. A fit to solely H1 and NMC data passes through the H1 points, but significantly undershoots the BCDMS data at the largest x values.

couplings v, a to the Z boson, on the longitudinal electron beam polarization (λ) and on the propagators via $\kappa = Q^2/[4\sin^2\theta_W \cos^2\theta_W (Q^2 + M_Z^2)]$, where θ_W is the electroweak mixing angle. They are built from the five genuine structure functions $(F_2, G_2, H_2, G_3, H_3)$ defined in Section 1, Eqs. (2) and (3) [11]:

$$\mathbf{F_2^{\pm}} = F_2 + \kappa(-v \mp \lambda a)G_2 + \kappa^2(v^2 + a^2 \pm 2\lambda a v)H_2 \quad (6)$$

$$\mathbf{xF_3^{\pm}} = \kappa(\lambda v \pm a)xG_3 + \kappa^2(-\lambda(v^2 + a^2) \mp 2av)xH_3 \ . \quad (7)$$

The $\mathbf{xF_3}$ term (proportional to Y_-) contributes sizeably only at large y and high Q^2. The high Q^2 NC cross sections measured currently at HERA for $\lambda = 0$ are approximately given by

$$\sigma^{\pm} \simeq Y_+ \cdot F_2 \ \pm \ \kappa a Y_- \cdot xG_3. \tag{8}$$

This causes a positive charge asymmetry between electron and positron scattering which is proportional to aa_q. This is a parity conserving effect which is determined by the function xG_3, measured previously by BCDMS at lower Q^2 for an isoscalar target (Fig. 1).

The H1 Collaboration has performed measurements of double differential NC scattering cross sections [47] using 35.6 pb^{-1} of e^+ data [46] taken in 1994-97 at $E_p =$ 820 GeV and 15 pb^{-1} of e^- data [47] taken in 1998-99 at $E_p = 920$ GeV. A comparison of the cross section measurements with electrons and positrons is illustrated in Fig. 9, which agrees with the expectation based on the γZ interference in NC scattering.

3 Light quark and charm quark distributions

3.1 Charged currents and up and down quarks

New information on the up and down quark distributions became available from improved measurements of the charged current cross section at HERA by H1 and ZEUS. The double-differential CC scattering cross section is given as

$$\frac{d^2\sigma^{\pm}_{cc}}{dxdy} = \frac{G^2}{2\pi} \cdot \left(\frac{M_W^2}{Q^2 + M_W^2}\right)^2 \cdot s\frac{1 \pm \lambda}{2} \cdot [Y_+ W_2^{\pm} \mp Y_- x W_3^{\pm}] \ , \tag{9}$$

where G is the Fermi constant and M_W the mass of the W boson. The CC cross section contains two structure functions for a given lepton beam charge and is proportional to s. The HERA energy is equivalent to a 53.9 TeV neutrino beam energy in a neutrino-nucleon fixed target experiment. The energy dependence is damped for $Q^2 \geq M_W^2$. In the QPM, the CC structure functions are combinations of up and down quark distribution sums, *i.e.*, $W_2^+ = D + \overline{U}$, $W_2^- = U + \overline{D}$, $xW_3^+ = D - \overline{U}$, and $xW_3^- = U - \overline{D}$ with $U = x(u + c)$ and $D = x(d + s)$. At large x ($x > 0.3$), the valence quark distributions u_v and d_v dominate the interaction cross sections, *i.e.*,

$$\sigma(e^+p \to \overline{\nu}X) \ \propto \ \overline{U} + (1-y)^2 D \to (1-y)^2 x d_v \tag{10}$$

$$\sigma(e^-p \to \nu X) \ \propto \ U + (1-y)^2 \overline{D} \to \qquad x u_v \ , \tag{11}$$

for $x \to 1$. A complete set of double differential $e^{\pm}p$ CC cross section data was presented by H1 using 36 pb^{-1} of positron-proton data (1994-1997) [46] and 15 pb^{-1} of electron data (1998-1999) [47]. The u dominated e^-p cross section was found

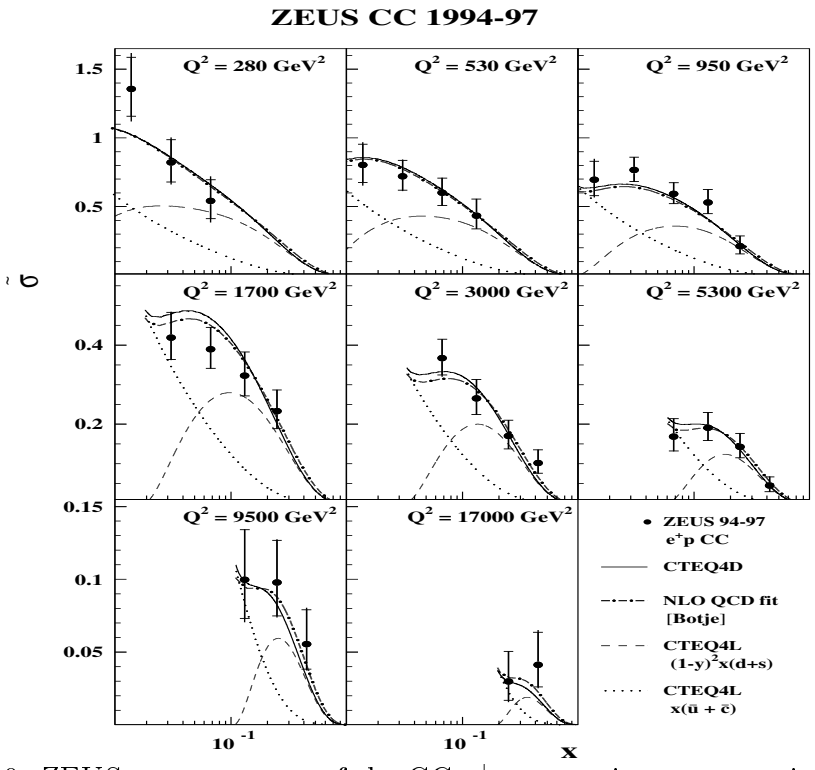

Figure 10: ZEUS measurement of the CC e^+p scattering cross section compared with $\overline{U}$ and D quark distributions, see Eq. 11, and different QCD fits.

to be about 5 times larger than the e^+p cross section at $Q^2 \simeq 10,000$ GeV^2. The e^+p CC data of H1 are consistent with the published measurement of the ZEUS Collaboration [49] based on 47.7 pb^{-1} (Fig. 10). The NC and CC measurements at high Q^2 are of particular interest for the determination of the d/u ratio at high x because their interpretation is free of nuclear corrections. Yet, an order of magnitude increase in luminosity is still required to access the high x region which represents one of the goals of the HERA luminosity upgrade program.

Deuterium binding corrections were recently reconsidered, and d_v was adjusted to be larger than previously assumed [51], the ratio d_v/u_v for $x \to 1$ tending to 0.2. An enlarged d quark distribution fits to the $W^\pm$ charge asymmetry data in $p\overline{p}$ collisions. Violation of u and d quark symmetry in protons and neutrons, however, which was suggested to explain the difference between the CCFR and NMC F_2 data [52], leads to too large a W asymmetry [53].

3.2 Sea quarks

Interesting data have become available on the flavor asymmetry in the nucleon sea. From a high statistics measurement of Drell-Yan muon pair production in pp and

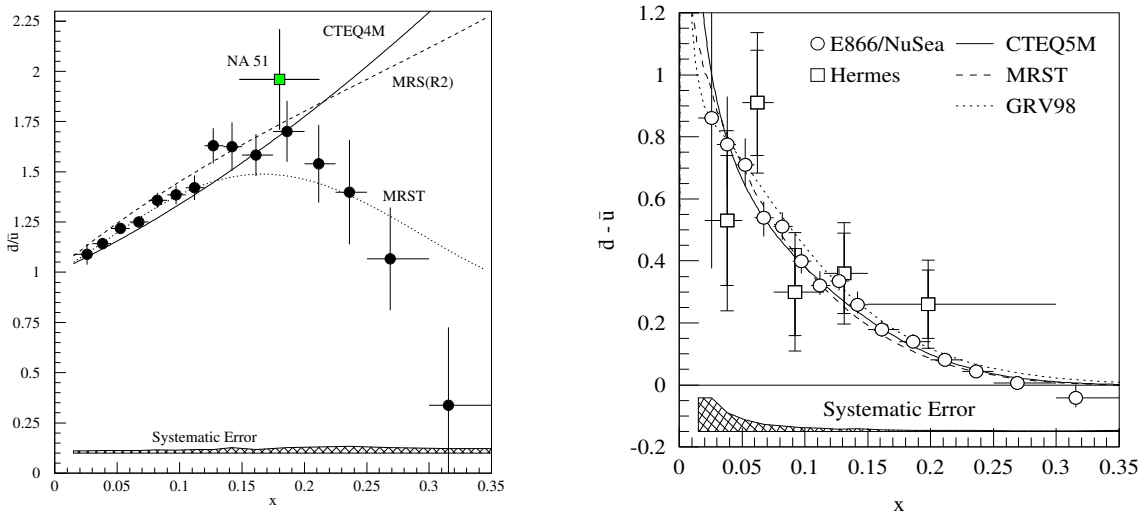

Figure 11: Measurements of $\overline{d}/\overline{u}$ and of $\overline{d}$ -$\overline{u}$ by NA 51, E866/NuSea and by HERMES compared with recent structure function fits.

pd collisions at the Tevatron, the E866/NuSea Collaboration obtained for $\int_0^1(\overline{u}-\overline{d})dx$ a value of -0.118 ± 0.011 at $\langle Q^2\rangle = 54$ GeV ^{2} [54]. This confirms and also significantly improves the previous NMC result of -0.15 ± 0.04 which was derived from a measurement of the Gottfried sum rule $\int_0^1[(F_2^p - F_2^n)/x]dx = 1/3 + 2/3 \cdot \int_0^1(\overline{u}-\overline{d})dx$. The measured ratio $\overline{d}/\overline{u}$ as a function of x is shown in Fig. 11. The data have considerable impact on global parametrizations of parton distributions. A consistent result, albeit of less statistical accuracy, was obtained by the HERMES Collaboration [55] with a measurement of semi-inclusive $\pi^{\pm}$ production in unpolarized ep and ed scattering at lower $\langle Q^2\rangle = 2.3$ GeV^2. A violation of flavor symmetry is not predicted in perturbative QCD, which points to non-perturbative effects such as Pauli blocking and pion clouds. In the latter model, the nucleon is expanded in a Fock state of mesons and baryons. Phenomenologically, one finds more π^+ than π^- in the nucleon, with a momentum distribution peaking at $x_\pi \simeq 0.2$ [56].

The NuTeV Collaboration [57] determined the strange quark distribution to be about half of the averaged nucleon sea, *i.e.* $s = [0.42 \pm 0.07(syst) \pm 0.06(stat)] \cdot (\overline{u}-\overline{d})/2$, in agreement with previous analyses of dimuon production in neutrino-nucleon scattering experiments.

Indications for a difference of the strange and anti-strange quark distributions at

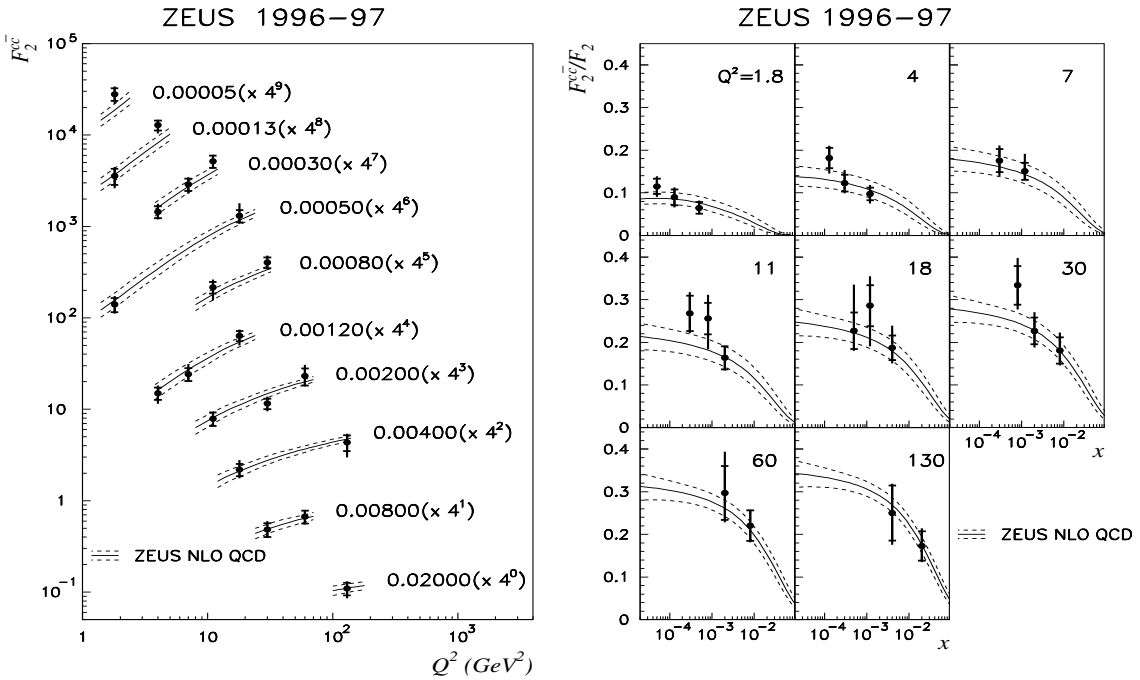

Figure 12: Measurement of $F_2^{c\bar{c}}(x,Q^2)$ and of the ratio $F_2^{c\bar{c}}/F_2$ in ep scattering at HERA by the ZEUS Collaboration with 37 pb^{-1} of data. The dashed error bands denote the uncertainty of the QCD fit which is dominated by the charm quark mass range chosen to be 1.2 to 1.6 GeV.

large $x \simeq 0.6$ were obtained in a recent reanalysis and global fit of DIS and Drell-Yan data [38]. Sensitivity to $(s-\overline{s})$ in this analysis comes from the CDHS data measuring $\sigma^{\nu} - \sigma^{\overline{\nu}} \sim x(s-\overline{s}) + Y_x(u_v + d_v)$ at high x. Such a strange asymmetry is possible in models considering states as $K^+\Lambda$ to be intrinsic to the nucleon where K^+ yields $\overline{s} \sim (1-x)$ and Λ yields $s \sim (1-x)^3$ [58].

3.3 Charm

Charm, as Witten already noticed in 1976, may "subject non-Abelian theories to a rigorous experimental test by measuring the charmed quark contribution to structure functions" [59]. Since then, the charm and beauty treatment in perturbative QCD has been worked out to higher orders [60]. Variable flavor schemes are being studied [61] to correctly handle the heavy flavor contributions near and beyond threshold in analyses of parton distributions, of the gluon distribution, and of α_s. A new measurement of the charm structure function $F_2^{c\bar{c}}$ was performed by the ZEUS Collaboration [62] using the ΔM tagging technique for $D^* \to K2\pi$ and $K4\pi$ (Fig. 12). The relative contribution of charm is large, reaching 30% at low x ($x < 0.001$) for $Q^2 \simeq 100$ GeV^2.

This large fraction is due to photon-gluon fusion as the dominant process for charm production. Further experimental progress at HERA towards high precision will be achieved with new or upgraded Silicon vertex detectors, higher luminosity, inclusion of further final states, and dedicated track triggers.

4 Gluon distribution and coupling constant α_s

4.1 Scaling violations at low x

Scaling violations in the DIS Q^2 region down to low $x \simeq 0.00005$ can be successfully described in the DGLAP formalism. This is again demonstrated with the new precise cross section measurement of H1 (Fig. 5). Conventional QCD fits use parametrizations of parton distributions at a starting scale Q_o^2 and evolve them in Q^2 to the highest Q^2 values up to order α_s^2. However, the splitting functions have expansions which contain also powers of $\ln(1/x)$. These are large at low x, such that $\alpha_s \ln(1/x) \simeq 1$, and yet do not seem necessary to phenomenologically describe the observed structure function behavior. Calculations are performed in order to account for these $\ln(1/x)$ terms [20] and to perhaps cure the instability of the BFKL equation in NLO [63]. Indications were reported for the presence of $\ln(1/x)$ terms in inclusive DIS data [64]. Experimentally, even higher precision is both required and possible for the structure function measurements, including F_L, which may lead to crucial tests of QCD at low x. Due to unitarity constraints, one expects to find saturation of the rising behavior of F_2 which, however, seems to be beyond the low x range accessible by HERA in the DIS region.

Scaling violations are conveniently studied using the $\ln Q^2$ derivative of F_2. In Fig. 13, the structure function F_2 from H1 is shown as a function of Q^2 for $x < 0.01$. The $\ln Q^2$ dependence is non-linear and can be described well by a quadratic expression $P_2 = a + b \ln Q^2 + c(\ln Q^2)^2$ (solid lines), which nearly coincides with the NLO QCD fit (dashed lines). The local derivatives $\partial F_2 / \partial \ln Q^2$ determined from the new H1 F_2 data are not constant in Q^2 and also depend on x. They can be described approximately for each bin of x by $b + 2 \cdot c \ln Q^2$. Small deviations from this behavior occur in NLO QCD. Using this expression, the derivatives are determined at fixed Q^2 and displayed as functions of x in Fig. 13. There is no departure observed from a rising behavior of the $\ln Q^2$ derivatives down to $Q^2 = 3$ GeV^2. If such a plot is made as a one-dimensional distribution, using the derivatives calculated for each bin of x at the mean Q^2 of a given bin, then the derivative $dF_2/d\ln Q^2$ flattens starting at $Q^2 \simeq 6$ GeV^2 [65]. In the region covered by the H1 data, this behavior reflects the restriction of the kinematic range of the measurement. Some analyses of the ZEUS data extending to lower $Q^2 \simeq 1$ GeV^2 introduce screening corrections in order to describe the behavior of F_2 [66, 67]. Both F_2 and F_L in this region should be measured with still higher accuracy (see Section 2.1.) as these functions

permit important information to be deduced on the dynamic interplay of gluon and sea distributions, on the effect of higher order and power corrections and on the shadowing phenomenon.

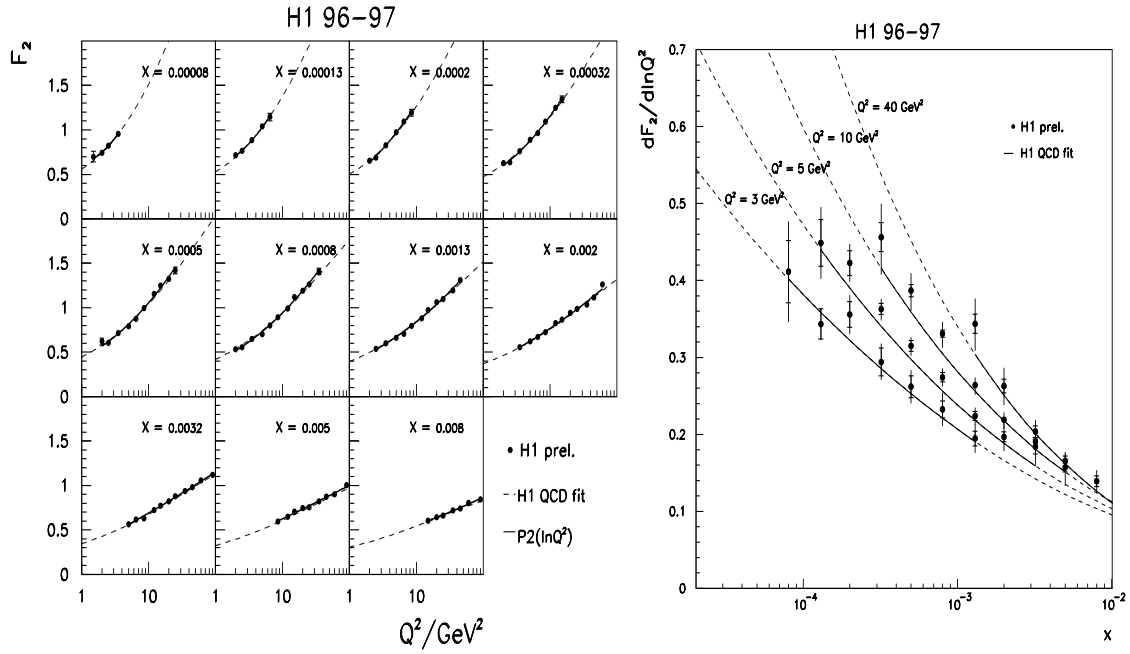

Figure 13: New preliminary H1 data show $F_2(x, Q^2)$ to be non-linear in $\ln Q^2$ at low x (left). The derivative $\partial F_2 / \partial \ln Q^2$ is a continuously falling function of x for $Q^2 \geq 3$ GeV^2 (right).

4.2 Gluon distributions

In QCD, the Q^2 evolution of F_2 is governed by the strong interaction coupling constant α_s. The evolution relates the quark distributions to the gluon distribution xg. The H1 Collaboration has performed a new NLO QCD fit to the H1 and NMC inclusive cross section data. It uses the DGLAP evolution equations for three light flavors with the charm and beauty contributions added according to the NLO calculation of the boson-gluon fusion process [68]. The proton structure function F_2 is a superposition of two independent functions with different evolutions, *i.e.* $F_2 = 5/18 \cdot S + 1/6 \cdot N$, where the singlet function $S = U + D$ is the sum of up and down quark distributions and the non-singlet function $N = U - D$ is their difference. In the new H1 fit, a different linear combination is introduced such that $U = 2/3 \cdot V + A$ and $D = 1/3 \cdot V + A$. In a simplified parton model ansatz with $\overline{u} = \overline{d}$ and $s + \overline{s} = (\overline{u} + \overline{d})/2$ one finds, $V = 3/4 \cdot (3u_v - 2d_v)$. This allows the quark counting rule to be applied, which constrains $\int V dx = 3$. This ansatz is used to fit the cross section data, Fig. 5, for $3.5 \leq$

$Q^2 \leq 3000$ GeV^2, assuming $\alpha_s(M_Z^2) = 0.118$. It is written in the $\overline{MS}$ renormalization scheme and generalized to account for the measured difference $\overline{u} - \overline{d}$ and the fraction of strange quarks, as discussed in Section 3. The salient feature of this new analysis is that it applies to DIS proton data only, but correctly determines the gluon momentum fraction to be about 0.45 at $Q^2 = 10$ GeV^2. The gluon distribution resulting from this fit is shown in Fig. 14 (left). The inner error band defines the experimental uncertainty of a few per cent at low x using the treatment of correlated systematic errors of [69]. The outer error band comprises uncertainties due to dependencies on the fit parameters $(Q^2_{min}, Q^2_o, \alpha_s, m_c)$ and on the choice of parametrizations for the initial distributions. A remarkable feature of xg is the crossing point at $x \simeq 0.06$ which is analogous to the Bjorken scaling behavior of F_2 and reflects the conservation of the gluon and quark momenta. In Fig. 14 (right), the gluon distribution is seen to

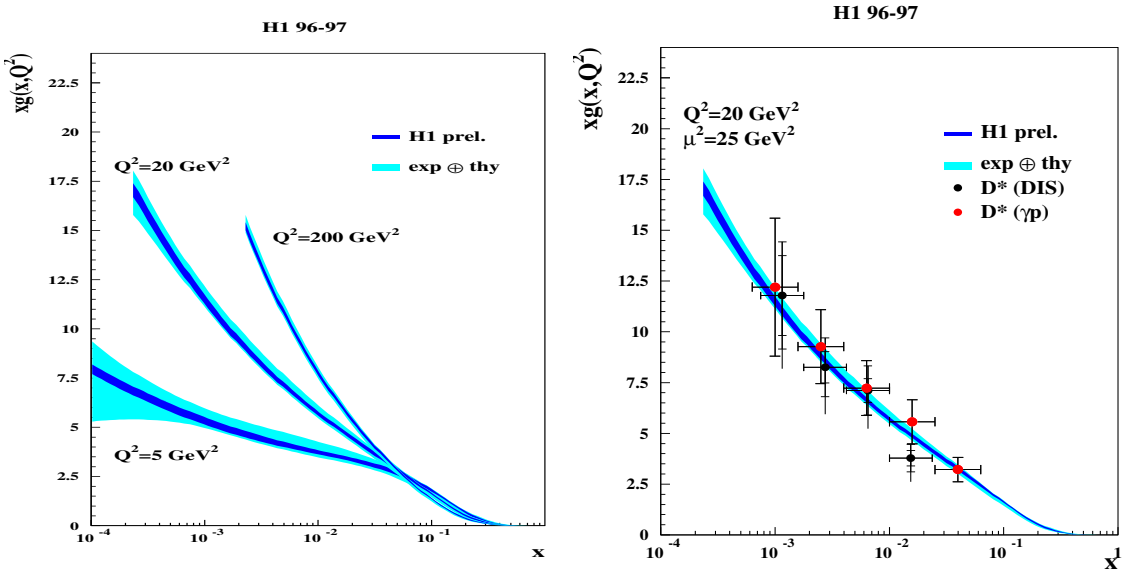

Figure 14: Determination of xg by H1 using NMC and H1 lp data in NLO QCD (left). Comparison of xg from scaling violations with the unfolded gluon distribution from charm D^* measurements by H1 (right).

agree very well with xg unfolded from the charm structure function in DIS and the photoproduction data of H1 [70]. This confirms hard scattering factorization. It has been recognized for some time that, in photoproduction ($Q^2 \simeq 0$), the charm mass provides a hard scale [71].

While xg at low x is well determined by the HERA structure function measurements, there are sizeable uncertainties of one order of magnitude at high $x \simeq 0.6$ [72]. The gluon distribution is accessed at high x by quark-gluon Compton scattering, leading to direct photon emission [73]. In a recent experiment by the E706 Collaboration, the photon p_T spectrum was found to exceed the QCD expectation by a

factor of about two. This has been cured phenomenologically by a Gaussian transverse momentum smearing with k_T of 1 GeV, larger than the intrinsic k_T value of about 0.4 GeV [74]. High E_T jet data at large rapidities are sensitive also to xg at large x and lead to a rather high gluon distribution. Inclusion of different data sets yields remarkably differing results. Resolving the issue of xg at high x is essential for a reliable prediction of Higgs production in pp colliders. It is necessary because the high x exponent c_g of $xg \propto (1-x)^{c_g}$ is known to be correlated with α_s. In this respect, precision measurements of structure functions at high x are important. Because F_2 vanishes as $(1-x)^3$, any measurement error at large x is amplified like $1/(1-x)$. The HERA collider experiments with their unique possibility to overconstrain the kinematics can be expected to lead to precision data also at high x [75] when the luminosity is upgraded.

Recently, updates of the GRV parametrizations were presented [76]. New sets of fits were made by the MRST [77] and the CTEQ groups [78]. GRV98 uses DIS, n/p, and Drell-Yan data assuming $\alpha_s(M_Z^2)$=0.114. MRST99 uses direct photon data of the WA70 experiment for different k_T and varies the d/u ratio, α_s, and m_c. CTEQ5 does not use direct photon data, but analyzes high E_T jet data instead. Sets are provided for different renormalization schemes and heavy quark treatments. As a consequence, there exists a variety of parametrizations illustrating the still large flexibility of theoretical assumptions and pointing to possible experimental contradictions. An interesting attempt was made recently [79] to quantify the experimental uncertainties of parton distributions resulting from global QCD fits to DIS data.

4.3 Determinations of α_s

New determinations of $\alpha_s(M_Z^2)$ with structure function data were presented recently. Conventional analyses parameterize a set of input quark distributions and xg at certain input scale Q_o^2 using the DGLAP equations to NLO to calculate the theoretical expectation. Minimization of a χ^2 function determines α_s and the roughly 10-15 parton distribution parameters. The treatment of systematic errors affects both the central value and the error size of $\alpha_s(M_Z^2)$. At low Q^2, power corrections to the logarithmic evolution may be sizeable and anticorrelate with α_s. Because analyses differ in these assumptions and use different sets of data, one may not be surprised to still find some spread of the quoted values of $\alpha_s(M_Z^2)$. Using the SLAC, BCDMS, and NMC p and n structure function data and taking into account systematic error correlations and higher twists $\propto 1/Q^2$, a value of $\alpha_s(M_Z^2)= 0.1183 \pm 0.0021(exp) \pm 0.0013(th)$ has been derived [80]. A similar analysis [81] including the published HERA data and adding all errors in quadrature yields $\alpha_s(M_Z^2)= 0.114 \pm 0.002(exp)^{+0.006}_{-0.004}(th)$, which is closer to a previous determination of $\alpha_s(M_Z^2)$ based on SLAC and BCDMS data [82]. The quoted theoretical errors represent the uncertainties of the renormalization scale μ_r. The former analysis compensates part of the μ_r dependence with a higher twist

contribution.

The theoretical uncertainties are diminished in NNLO calculations. So far only partial results are available on the 3-loop splitting functions, while the β function and the coefficient functions are known [83]. This has given rise to a revival of moment analyses. In [84] the xF_3 data of the CCFR Collaboration are reconstructed using orthogonal Jacobi polynomials. Power corrections are considered and a value of $\alpha_s(M_Z^2)= 0.118 \pm 0.002\ (stat)\ \pm 0.005\ (syst)\ \pm 0.003\ (th)$ is obtained in NNLO corresponding to 0.120 in NLO. While this uses a pure non-singlet function, not coupled to the gluon distribution, a new analysis of SLAC, BCDMS, NMC, ZEUS, and H1 data using Bernstein polynomials of F_2 yields $\alpha_s(M_Z^2)= 0.1163 \pm 0.0023$ in NNLO with a single error supposed to comprise all experimental and theoretical uncertainties. This analysis [85] is extended to a Q^2 range of 2.5 to 230 GeV^2 and includes power corrections. Its NLO result is 0.1175, and moments of xg are determined.

Although all these analyses represent quite remarkable theoretical and experimental progress, one still has to be cautious. The treatments of systematic error in these analyses differ. An important issue is the possible incompatibility of different data sets. For example, the combination of SLAC and BCDMS data yields an $\alpha_s(M_Z^2)$ value near to 0.114. Yet, this is known to result from a superposition of the BCDMS data favoring a value of about 0.110 with the SLAC data preferring $\alpha_s \simeq 0.120$. Furthermore, the moment analyses, while theoretically advanced to NNLO, shift the data weight to large x where the accuracy of the data is less impressive. Moreover, there is a dependence of the result on the minimum Q^2 considered [81] which often leads to the introduction of power corrections with phenomenological x dependence. Finally the likely presence of $\ln(1/x)$ terms will affect the data interpretation. It is thus concluded that the great potential of DIS data to determine $\alpha_s(M_Z^2)$ still requires much more work in order to determine α_s at the one per cent level of accuracy.

Interesting ideas are pursued to replace in the QCD analysis xg by the derivative $\partial F_2/\partial \ln Q^2$ [81, 86] and to develop the method of truncated moments [87] in order to avoid the low x region in analyses of structure functions other than F_2. The approach of double asymptotic scaling at low x of F_2 [15] represents a three parameter solution of the DGLAP equations and may lead to a particularly accurate determination of $\alpha_s(M_Z^2)$ [88, 89]. This solution predicts a steady increase of xg towards low x which yet has to be damped at certain x and Q^2 because xg may not exceed the proton size πr_p^2 by too large an amount [90].

5 On the future of deep inelastic scattering

During the year 2000, the HERA luminosity will be upgraded [91] in order to provide an integrated luminosity of 150 pb^{-1} per year. Variations of proton and electron beam energies and the use of electron polarization in colliding mode will further

enable the electroweak structure function measurements and enhance the discovery potential of the machine. The modifications of HERA are accompanied by major detector upgrades of the luminosity, forward tracking, and Silicon vertex detectors of H1 and ZEUS.

The main injector neutrino oscillation detector at Fermilab (MINOS-near) will lead to precise, high statistics data ($4 \cdot 10^7$ events/year) on the six structure functions (F_2, xF_3, and F_L for νFe and $\overline{\nu} Fe$ scattering). This is necessary to disentangle the nucleon sea, *i.e.*, to measure $\overline{u} + \overline{d}$, c, and s [92]. Measurements of the nuclear dependence of neutrino DIS cross sections using additional targets will determine νA shadowing and perhaps help in resolving the CCFR-NMC puzzle described in Section 2.2. An increase of neutrino energy by a factor of 10 would be possible in a 250 GeV muon storage ring providing extremely intense neutrino beams [93, 94].

The obvious next step in electron-proton DIS is a new ep machine [95]. The

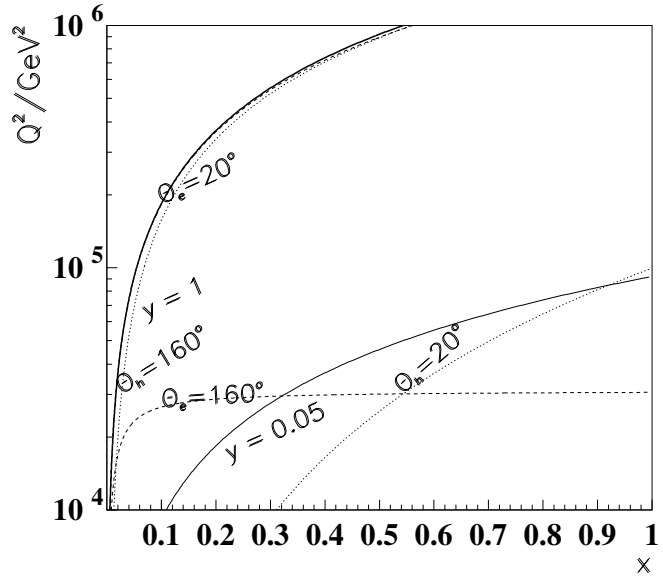

Figure 15: Kinematic region of a possible future ep collider using 500 GeV electrons from TESLA and 920 GeV protons from HERA. The line $y = 0.05$ represents the upper kinematic limit of ep collisions in HERA. Because the THERA machine is symmetric in energy, it provides full containment of highly energetic electrons and hadrons at large x and high Q^2 as indicated with the iso-θ lines at 20^o and 160^o.

proposed linear collider at DESY, TESLA, may provide collisions of electrons of up to about 500 GeV against HERA protons of nearly 1 TeV. A similar energy of $\sqrt{s} \simeq 1.5$ TeV can be obtained in ep collisions at LEP-LHC energies. These machines differ in technology, luminosity, and kinematics. Yet one can envisage extending the low x acceptance by a factor of 20 and DIS data to $Q^2 \simeq 500,000$ GeV^2 and beyond, (Fig. 15). Saturation and sub-structure will be searched for in this extended range.

Thirty years after the pioneering SLAC ep experiments, deep inelastic scattering still has an exciting future.

6 Concluding remarks

HERA has opened the field of low x physics which is governed by gluon interactions and which is far from being fully understood. The gluon momentum density at low x is very large. This causes the structure function F_2 to rise at low x. It determines the longitudinal structure function to be large and the production cross section of heavy flavors to be sizeable. Increasing experimental precision leads to sensitive tests of QCD at higher orders perturbation theory. The most accurate determinations of the gluon distribution *and* the strong interaction coupling constant are within reach with DIS data. Electroweak neutral and charged current structure functions provide new insights in the proton structure at high x. Measurements at $Q^2 \simeq M_Z^2$ probe the proton nearly 100 times below the parton level reached three decades ago. It is a spectacular result that no substructure of leptons or quarks has been observed so far. At the same time, significant progress is made with various fixed target and pp experiments leading to deeper insight in the partonic structure of the proton. The gluon distribution at large x is small, but remains to be determined. The next step is tests of the inner proton structure down to $2 \cdot 10^{-19}$m. The outcome is unknown, and deep inelastic physics is therefore worth continuing effort.

It is a pleasure to thank John Jaros and co-organizers for an excellent Symposium. Many thanks are due to colleagues from the various DIS experiments for providing information and guidance in understanding their results. I have to thank too many individuals to be named here, members of the H1 Collaboration and its structure function group, physicists, and engineers of the Zeuthen Silicon detector group, colleagues in the DIS99 conference committees, many theoretical and experimental physicists for useful discussions and for reading the manuscript, and also several well-known physicists of the BCDMS Collaboration who introduced me to deep inelastic scattering years ago. Modern particle physics is a huge common effort of a large, mostly friendly community. Particular recognition is due to the youngest: I sincerely thank Vladimir Arkadov, Doris Eckstein, Alexander Glazov, and, in particular, Rainer Wallny for efficient help in preparing this talk and exciting moments of joint research.

References

[1] E. D. Bloom *et al.*, Phys. Rev. Lett. **23**, 930 (1969); M. Breidenbach *et al.*, Phys. Rev. Lett. **23**, 935 (1969).

[2] M. Yearin and R. Hofstadter, Phys. Rev. **110**, 552 (1958).

[3] R. P. Feynman, Phys. Rev. Lett. **23**, 935 (1969).

[4] J. Bjorken, Phys. Rev. **179**, 1547 1969.

[5] J. Bjorken and E. A. Paschos, Phys. Rev. **185**, 1975 1969.

[6] D. J. Fox *et al.*, Phys. Rev. Lett. **33**, 1504 (1974).

[7] D. J. Gross and F. Wilczek, Phys. Rev. **D 9**, 980 (1974); H. Georgi and H. D. Politzer, Phys. Rev. **D 9**, 416 (1974).

[8] For a review see: P. Gallison, Rev. Mod. Phys. **55**, 477 (1983).

[9] C. Y. Prescott *et al.*, Phys. Lett. **B 77**, 347 (1978).

[10] E. Derman, Phys. Rev. **D 7**, 2755 (1973).

[11] M. Klein and T. Riemann, Z. f. Phys. **C 24**, 151 (1984).

[12] A. Argento *et al.* [BCDMS Collaboration], Phys. Lett. **140 B**, 142 (1984).

[13] I. Abt *et al.* [H1 Collaboration], Nucl.Phys. **B 407**, 515 (1993).

[14] M. Derrick *et al.* [ZEUS Collaboration], Phys. Lett. **B 316**, 412 (1993).

[15] A. De Rujula *et al.*, Phys. Rev. **D 10**, 1649 (1974).

[16] G. Parisi and R. Petronzio, Phys. Lett. **62 B**, 331 (1976); V. Novikov *et al.*, JETP Lett. **76**, 341 (1976); M. Glück and E. Reya, Nucl. Phys. **B 130**, 76 (1977).

[17] M. Glück, E. Reya and A. Vogt, Z. f. Phys. **C 53**, 127 (1992).

[18] J. Blümlein, in Proceedings of the Ringberg Workshop "Trends in HERA Physics 1999", eds. G. Grindhammer, B. Kniehl and G. Kramer, Springer, Berlin 1999, hep-ph/990949 (1999) and references therein.

[19] P. Marage, Invited Talk, Proceedings of the EPS Conference, Tampere, Finland, 1999, to appear.

[20] G. Altarelli, R. Ball and S. Forte, CERN-Th/2000-010, hep-ph/00001157.

[21] Proceedings of the 7th International Workshop on Deep Inelastic Scattering and QCD, Nucl. Phys. B (Proc. Suppl.) **79** (1999), ed. by J. Blümlein and T. Riemann.

[22] V. Shekelyan, in Proceedings of the 1997 International Symposium on Lepton-Photon Interactions, A. De Roeck and A. Wagner, eds. (World Scientific, Singapore, 1998).

[23] A. Levy, The Structure of the Troika, TAUP 2531, hep-ph/9811462.

[24] A. Donnachie and P. V. Landshoff, Phys. Lett. **B 437**, 408 (1998);
P.V. Landshoff in [21], p. 204.

[25] C. Amelung, in [21], p. 176 (1999).

[26] J. J. Sakurai and D. Schildknecht, Phys. Lett. **B 40**, 121 (1972).

[27] H. Abramowicz and A. Levy, DESY preprint 97-251 (1997).

[28] E. Bloom and F. Gilman, Phys. Rev. **D 4**, 2901 (1971).

[29] C. Keppel, in [21], p. 182 (1999).

[30] A. De Rujula, H. Georgi and H. D. Politzer, Ann. Phys. **103**, 3115 (1977).

[31] W. Seligman *et al.* [CCFR Collaboration], Phys. Rev. Lett. **79**, 1213 (1997).

[32] M. Vakili *et al.* [CCFR Collaboration], hep-ex/9905052 (1999).

[33] A. C. Benvenuti *et al.* [BCDMS Collaboration], Z. f. Phys. **C 63**, 29 (1994).

[34] IHEP-JINR Collaboration, hep-ex/9905038 (1999); A.V. Sidorov *et al.*, in [21], p. 99 (1999).

[35] A. T. Doyle, in Proceedings of the 1998 International Conference on High Energy Physics, A. Astbury, D. Axen and J. Robinson, eds. (World Scientific, Singapore, 1999).

[36] U. K. Yang [CCFR Collaboration], private communication.

[37] F. Boros *et al.*, Phys. Lett. **B 468**, 161 (1999).

[38] V. Barone, C. Pascaud and F. Zomer, hep-ph/9907512 (1999).

[39] R. Gandhi *et al.*, Phys. Rev. **D 58**, 093009 (1998).

[40] M. Glück, S. Kretzer and E. Reya, Astro. Part. Phys. **11**, 327 (1998).

[41] J. Kwiecinski, A. D. Martin and A. M. Stasto, hep-ph/9905307 (1999).

[42] U. K. Yang *et al.* [CCFR Collaboration], in [21], p. 89 (1999).

[43] K. Ackerstaff *et al.* [HERMES Collaboration], hep-ex/9910071 (1999).

[44] M. Klein [H1 Collaboration], in Proceedings of the 1998 International Conference on High Energy Physics, A. Astbury, D. Axen and J. Robinson, eds. (World Scientific, Singapore, 1999).

[45] E. Zijlstra and W. van Neerven, Nucl. Phys. **383**, 525 (1992).

[46] C. Adloff *et al.* [H1 Collaboration], DESY 99-107, hep-ex/9908059 (1999), Eur. Phys. J. to appear.

[47] H1 Collaboration, Paper no. 157b, submitted to the 1999 EPS High Energy Physics Conference.

[48] J. Breitweg *et al.* [ZEUS Collaboration], DESY 99-056 (1999).

[49] J. Breitweg *et al.* [ZEUS Collaboration], DESY 99-059 (1999).

[50] J. Breitweg *et al.* [ZEUS Collaboration], Papers no. 1549 and 558, submitted to the 1999 EPS High Energy Physics Conference.

[51] A. Bodek and U. K. Yang, Phys. Rev. Lett. **82**, 2467 (1999).

[52] C. Boros, J. T. Lonergan and A. W. Thomas, Phys. Rev. Lett. **81**, 4075 (1998).

[53] A. Bodek, in [21] p. 137 (1999).

[54] R. Towell [NuSea Collaboration], in Proceedings of the 1999 EPS High Energy Physics Conference.

[55] C. A. Miller, in [21], p. 146 (1999).

[56] A. Szczurek and V. Uleshchenko, in [21], p. 149 (1999) and references therein.

[57] T. Adams *et al.* [NuTeV Collaboration], hep-ex/9906038 (1999).

[58] W. Melnitchouk, hep-ph/9906488 (1999) and references cited therein.

[59] E. Witten, Nucl. Phys. **104**, 445 (1976); M. A. Shifman, A. I. Vainshtein and V. I. Zakharov, Nucl. Phys. **136**, 157 (1978); M. Glück and E. Reya, Phys. Lett. **B 83**, 999 (1979).

[60] J. Smith, in [21], p. 124 (1999) and references therein; for a review see: W. van Neerven, Lecture at the Zakopane Winter School, 1998.

[61] W. K. Tung, in Proceedings of the 5th International Workshop on Deep Inelastic Scattering and QCD, Chicago, IL (1997), p. 1410, ed. by J. Repond and D. Krakauer.

[62] J. Breitweg *et al.* [ZEUS Collaboration], DESY 99-101, hep-ex/9908012 (1999).

[63] V. S. Fadin and L. N. Lipatov, Phys. Lett. **B429**, 127 (1998); M. Ciafaloni, in [21], p. 201 (1999) and references cited therein.

[64] R. S. Thorne, in [21], p. 210 (1999).

[65] A. Caldwell, talk at the DESY Theory Workshop, Hamburg, October 1997; J. Breitweg *et al.* [ZEUS Collaboration], Eur. Phys. J. **C 7**, 609 (1999).

[66] E. Gotsman, E. Levin and U. Maor, Nucl. Phys. **539**, 535 (1999).

[67] C. Merino, A. B. Kaidalov and D. Petermann, hep-ph/9911331 (1999).

[68] E. Laenen *et al.*, Nucl. Phys. **B 392**, 162 (1993); S. Riemersma, J. Smith and W. van Neerven, Phys. Lett. **B 347**, 143 (1995).

[69] C. Pascaud and F. Zomer, LAL Orsay preprint, LAL/95-05 (1995).

[70] C. Adloff *et al.* [H1 Collaboration], Nucl. Phys. **B 545**, 21 (1999).

[71] M. A. Shifman, A. I. Vainshtein and V. I. Zakharov, Phys. Lett. **65 B**, 255 (1976).

[72] M. Begel, in [21], p. 244 and references therein.

[73] F. Halzen and D. M. Scott, Phys. Rev. **D 22**, 1617 (1980).

[74] L. Apanasevich *et al.*, Phys. Rev. Lett. **81**, 2642 (1998).

[75] M. Botje, M. Klein and C. Pascaud, in Proceedings of the International Workshop on Future Physics at HERA, Hamburg 1996, Vol.1, p. 33, ed. by G. Ingelman, A. De Roeck and R. Klanner.

[76] M. Glück, E. Reya and A. Vogt, hep-ph/9806404 (1998).

[77] A. Martin *et al.*, hep-ph/9907231 (1999).

[78] H. L. Lai *et al.* [CTEQ Collaboration], hep-ph/9903282 (1999).

[79] M. Botje, in [21], p. 111 (1999).

[80] S. Alekhin, Phys. Rev. **D 59**, 114016 (1999).

[81] A. Vogt, in [21], p. 102 (1999).

[82] A. Milsztaijn and M. Virchaux, Phys. Lett. **B 274**, 221 (1992).

[83] W. van Neerven, in [21], p. 36 (1999).

[84] A. L. Kataev, G. Parente and A. V. Sidorov, hep-ph/9905310 (1999).

[85] J. Santiago and F. J. Yndurain, hep-ph/9907387 (1999).

[86] P. W. Johnson and W. Tung, Phys. Rev. **D16**, 2769 (1977).

[87] L. Magnea and S. Forte, hep-ph/9910421 (1999).

[88] R. D. Ball and S. Forte, Phys. Lett. **B 358**, 365 (1995).

[89] A. De Roeck, M. Klein and Th. Naumann, Phys. Lett. **B 385**, 411 (1996).

[90] E. Levin, DESY preprint 99-113, hep-ph/9908379 (1999).

[91] A. Wagner, in [21], p. 176 (1999).

[92] J. Morfin, in [21], p. 664 (1999).

[93] S. Geer, Phys. Rev. **D 57**, 1 (1998).

[94] B. King, in Proceedings of the Muon Collider Workshop, Fermilab, Nov. 1997, hep-ex/9907033 (1999).

[95] M. Tigner, B. H. Wiik and F. Willeke, in Proceedings of the 1990 Particle Accelerator Conference.